Supplementary Information for

Polarization-entangled photon-pair source with van der Waals 3R-WS_2 Crystal

Jiangang Feng[1, †], Yun-Kun Wu[2, 3, 4, †, *], Ruihuan Duan[5, †], Jun Wang[6], Weijin Chen[1], Jiazhang Qin[1], Zheng Liu[5], Guang-Can Guo[2, 3, 4], Xi-Feng Ren[2, 3, 4, *], Cheng-Wei Qiu[1, *]

[1] Department of Electrical and Computer Engineering, National University of Singapore, Singapore 117583, Singapore

[2] CAS Key Laboratory of Quantum Information, University of Science and Technology of China, Hefei 230026, China

[3] CAS Center for Excellence in Quantum Information and Quantum Physics, University of Science and Technology of China, Hefei 230026, China

[4] Hefei National Laboratory, University of Science and Technology of China, Hefei 230088, China

[5] School of Materials Science and Engineering, Nanyang Technological University, Singapore 639798, Singapore

[6] Department of Optical Science and Engineering, and Shanghai Frontiers Science Research Base of Intelligent Optoelectronics and Perception, Fudan University, Shanghai 200433, China

[†] These authors contributed equally to this work

Email: chengwei.qiu@nus.edu.sg (C.-W.Q.); renxf@ustc.edu.cn (X.-F.R.); wuyk123@mail.ustc.edu.cn (Y.-K.W.)

The PDF file includes:

1. Materials and methods

Material growth

3R-WS_2 bulk single crystals are synthesized using the chemical vapor transport (CVT) method. A stoichiometric mixture of W and S elements, supplemented with WCl_5 as a transport agent, is placed in a quartz tube. The quartz tube is then sealed under a vacuum ($<10^{-2}$ Pa) and transferred to a two-zone horizontal furnace. The furnace temperatures are set to 1050°C and 1000°C for the respective zones, maintaining this temperature gradient for 20 days. Following a 15-day cooling process, 3R-WS_2 bulk single crystals are obtained in the cold zone. The flakes of 3R-WS_2 are mechanically exfoliated onto glass substrates for optical measurements.

SHG measurements

SHG of 3R-WS_2 is excited using a Ti:sapphire femtosecond laser (Spectra-Physics) operating at a 1 kHz repetition rate and a pulse duration of 100 fs. The generated SHG photons are captured via a 50× microscope objective with a numerical aperture (NA) of 0.75. The SHG signals are then detected by an imaging spectrometer (HORIBA, iHR550) equipped with a liquid nitrogen-cooled charge-coupled device. For linear polarization-resolved measurements, a half-wave plate (HWP) is utilized to modulate the polarization state of the pump beam. A sequence of HWP and a linear polarizer serves as an analyzer, ensuring parallel polarization alignment between the pump and the analyzer. To address circular polarization-resolved measurements, we employ a combination of a HWP and a quarter-wave plate (QWP) to generate a circularly polarized pump beam. The circular polarization of the SHG signals is resolved using a set of QWP and linear polarizer. Wavelength-dependent SHG studies are conducted by pumping with a femtosecond laser beam, whose wavelength is tuned using an optical parametric amplifier (TOPAS, Spectra-Physics). To evaluate the second-order susceptibility $\chi^{(2)}$, we employ a 500 nm thick *x*-cut $LiNbO_3$ as a standard sample, with a *d* value of 40 pm V^{-1}. The SHG intensities of 3R-WS_2 and $LiNbO_3$ are recorded under the same excitation conditions, followed by the calculation of $\chi^{(2)}$ using the method reported in Ref. 4.

Quantum correlation measurements

The quantum correlation measurements are conducted on the setup sketched in Fig. 2A, ensuring consistent polarizations of signal and idler photons. A 457 nm continuous-wave laser beam is circularly polarized through a sequence comprising a polarizing beam splitter (PBS), a HWP, and a QWP. An additional HWP, positioned before the PBS, is employed to tune the pump power. This pump is then focused onto the sample via a 10× objective (NA = 0.25). The generated photon pairs are collected by a 50× objective (NA = 0.5) and subsequently projected into circularly polarized components using a QMP, a HWP, and a PBS. To filter out the pump light, a long-pass filter at 900 nm is used in conjunction with a band-pass fiber filter, which has a central wavelength of 925 nm and a linewidth of 50 nm. The photon pairs are then coupled into a multimode fiber and split using a 50:50 fiber beam splitter (Thorlabs, TG625R5F1A). Detection of the signal and idler photons is achieved via two single photon detectors (SCONTEL). Finally, the second-order correlation function and the coincidence of the twin photons are calculated using a time-correlated single photon counting (TCSPC) module (qutools quTAG). The coincidence window in measurements of coincidence rate and quantum tomography was set as 1 ns.

The detection efficiency for SPDC measurements can be determined using the following equation:

$$\eta = \eta_{i,s}^{Obj} \times \eta_{i,s}^{HWP} \times \eta_{i,s}^{QWP} \times \eta_{i,s}^{PBS} \times \eta_{i,s}^{Filter} \times \eta_{i,s}^{BS} \times \eta_{i,s}^{Fibre} \times \eta_{i,s}^{SPD} \tag{S2}$$

where $\eta_{i,s}^{Obj} = 0.7^2, \eta_{i,s}^{HWP} = \eta_{i,s}^{QWP} = 0.95^2$ are the twin photons transmission through the sequence of objectives, HWPs and QWPs, $\eta_{i,s}^{PBS} = 0.95^2$ is the efficiency of the polarizing beam splitters, $\eta_{i,s}^{BS} = 0.5 \times 0.98^2 = 0.48$ is the efficiency of beam splitter, $\eta_{i,s}^{Fibre} = 0.72^2$ is the efficiency of coupling the photons from free space into fibre, and $\eta_{i,s}^{SPD} = 0.38^2$ corresponds to the quantum efficiency of the single photon detectors at the degenerate twin photons wavelength 914 nm. The filter loss in our system originates from two aspects. First, the transmittance of filter is about 0.95. Second, we apply a long-pass filter at 900 nm and band-pass filter centered at 925 nm to enable quantum correlations. To evaluate this efficiency loss from bandwidth, we record the broadband coincidence rate using an 800 nm long-pass filter and finds a six-fold enhancement of coincidence rate. Therefore, our filter efficiency can be calculated as $\eta_{i,s}^{Filter} = 0.95^2 \times 0.95^2 \times 1/6 = 0.143$. Consequently, the overall detection efficiency of our system is calculated to be approximately 0.19%.

Quantum-state tomography

Quantum state tomography is the most common method to measure the density matrix $\hat{\rho}$ of a state. $\hat{\rho}$ is considered as a positive semidefinite Hermitian matrix with d^2 real variables, where d is the dimension of the matrix. For a *n*-qubits state, the dimension of the density matrix is 2^n, thus corresponding to 16 variables in our work. The polarization projected bases are $\{H, V, D, R\}^2$ in our experiments, in which $|H\rangle$ is the horizontally polarized state, $|V\rangle$ is the vertically polarized state, $|D\rangle = (|H\rangle + |V\rangle)/\sqrt{2}$ and $|R\rangle = (|H\rangle + i|V\rangle)/\sqrt{2}$, respectively. These 16 measured operators form a complete basis in the Hilbert space of the two-photon polarization state and 16 measured results are obtained. Therefore, solving the variables with the experimental results could reconstruct the measured parameterized density matrix. The maximum likelihood estimation method is used to solve the reconstruction equations against the experimental noise.

The experimental configuration for quantum-state tomography is illustrated in Fig. S5. This setup shares similarities with the pump and focusing components used in the quantum-correlation measurements. Following the filtering of the pump light, photon pairs are divided by a polarization-independent 50:50 beam splitter. Subsequently, signal and idler photons are individually projected into different polarization bases by employing a sequence of a QWP, a HWP, and a PBS. The photons are then directed into multimode fibers and detected by two single-photon detectors, following by analysis of coincidences using a TCSPC module.

2. Polarization dependence of SHG in 3R-WS_2

For second-order nonlinear process, nonlinear polarization $P_i^{2\omega}$ as a function of electric field $E_{i,j,k}$ can be written as,

$$P_i(2\omega) = \epsilon_0 \sum\nolimits_{jk} \chi_{ijk}^{(2)} E_j(\omega) E_k(\omega) \tag{S3}$$

where ϵ_0 is the permittivity of free space, $\chi_{ijk}^{(2)}$ is the second-order susceptibility, indices (i, j, k) run over coordinates (x, y, z). For 3R-WS_2 with a *R3m* space group and a C_{3v} point group, the nonvanishing elements in second-order susceptibility tensor are $\chi_{xzx}^{(2)} = \chi_{xxz}^{(2)} = \chi_{yzy}^{(2)} = \chi_{yyz}^{(2)}, \chi_{zxx}^{(2)} = \chi_{zyy}^{(2)}, \chi_{zzz}^{(2)}, \chi_{yyy}^{(2)} = -\chi_{yxx}^{(2)} = -\chi_{xxy}^{(2)} = -\chi_{xyx}^{(2)}$.

The notation can be simplified by introduce a 3×6 rank tensor d_{il}, where $\chi_{ijk}^{(2)} = 2d_{il}$, $l = 1, 2, 3, 4, 5, 6$ corresponds to $jk = xx, yy, zz, yz/zy, zx/xz, xy/yx$. For SHG, nonlinear polarization can be calculated by,

$$\begin{bmatrix} P_x(2\omega) \\ P_y(2\omega) \\ P_z(2\omega) \end{bmatrix} = 2\epsilon_0 \begin{bmatrix} d_{11} & d_{12} & d_{13} & d_{14} & d_{15} & d_{16} \\ d_{21} & d_{22} & d_{23} & d_{24} & d_{25} & d_{26} \\ d_{31} & d_{32} & d_{33} & d_{34} & d_{35} & d_{36} \end{bmatrix} \begin{bmatrix} E_x(\omega)^2 \\ E_y(\omega)^2 \\ E_z(\omega)^2 \\ 2E_y(\omega)E_z(\omega) \\ 2E_x(\omega)E_z(\omega) \\ 2E_x(\omega)E_y(\omega) \end{bmatrix} \tag{S4}$$

For 3R-WS_2 with x axis along zigzag direction, d_{il} tensor takes following form,

$$d_{il} = \begin{bmatrix} 0 & 0 & 0 & 0 & d_{31} & -d_{22} \\ -d_{22} & d_{22} & 0 & d_{31} & 0 & 0 \\ d_{31} & d_{31} & d_{33} & 0 & 0 & 0 \end{bmatrix} \tag{S5}$$

The nonlinear polarization in SHG process is given by,

$$\begin{bmatrix} P_x(2\omega) \\ P_y(2\omega) \\ P_z(2\omega) \end{bmatrix} = 2\epsilon_0 \begin{bmatrix} 2d_{31}E_x(\omega)E_z(\omega) - 2d_{22}E_x(\omega)E_y(\omega) \\ -d_{22}E_x(\omega)^2 + d_{22}E_y(\omega)^2 + 2d_{31}E_y(\omega)E_z(\omega) \\ d_{31}\left(E_x(\omega)^2 + E_y(\omega)^2\right) + d_{33}E_z(\omega)^2 \end{bmatrix} \tag{S6}$$

Linear polarization response. For a linearly polarized pump field in the form of $\boldsymbol{E} = E_0[\cos\theta \quad \sin\theta \quad 0]^{\mathrm{T}}$, the SHG intensity under a parallel linear analyzer can be expressed as,

$$I_{para}(\theta) = 4\epsilon_0^2 d_{22}^2 E_0^4 (\sin^3\theta - 3\cos^2\theta\sin\theta)^2 \tag{S7}$$

Circularly polarized pump. The circularly polarized pump is defined as $\boldsymbol{E} = E_0[1 \quad i\sigma \quad 0]^{\mathrm{T}}$, where $\sigma = \pm 1$ is spin angular momentum of light, corresponding to right/left-handed circular polarization. Then, nonlinear polarization can be calculated as,

$$\begin{bmatrix} P_x(2\omega) \\ P_y(2\omega) \\ P_z(2\omega) \end{bmatrix} = -4\epsilon_0 d_{22} E_0^2 \begin{bmatrix} 1 \\ -i\sigma \\ 0 \end{bmatrix} \tag{S8}$$

Therefore, circular polarization is flipped during SHG process in a nonlinear crystal with a C_{3v} point group.

3. Optical selection rule in SPDC process.

In SPDC process, the relationship between the idler polarization, and the pump and signal fields can be described as,

$$\begin{bmatrix} P_{ix} \\ P_{iy} \\ P_{iz} \end{bmatrix} = 4\epsilon_0 \begin{bmatrix} 0 & 0 & 0 & 0 & d_{31} & -d_{22} \\ -d_{22} & d_{22} & 0 & d_{31} & 0 & 0 \\ d_{31} & d_{31} & d_{33} & 0 & 0 & 0 \end{bmatrix} \begin{bmatrix} E_{px}E_{sx} \\ E_{py}E_{sy} \\ E_{pz}E_{sz} \\ E_{py}E_{sz} + E_{pz}E_{sy} \\ E_{px}E_{sz} + E_{pz}E_{sx} \\ E_{px}E_{sy} + E_{py}E_{sx} \end{bmatrix} \tag{S9}$$

where E_{sx}, E_{sy}, E_{sz} denote the x, y, z components of signal field, E_{px}, E_{py}, E_{pz} represent the electric field of pump. Under a circular polarization pump in the form of $\boldsymbol{E_p} = E_0[1 \quad i\sigma \quad 0]^{\mathrm{T}}$, the transverse polarization of idler can be written as,

$$\begin{bmatrix} P_{ix} \\ P_{iy} \\ P_{iz} \end{bmatrix} = 4i\epsilon_0 E_0 d_{22}\left(E_{sx} - i\sigma E_{sy}\right) \begin{bmatrix} 1 \\ -i\sigma \\ 0 \end{bmatrix} \tag{S10}$$

According to Eq. S9, signal and idler photons exhibit opposite spin angular momentum compared to pump photons.

4. Generation of Bell states using C_3 symmetric nonlinear crystals

The non-zero second-order nonlinear susceptibility tensors of a crystal with C_3 symmetry can be listed as follow:

$$\chi^{(2)} = \begin{bmatrix} \chi^{(2)}_{xxx} & \chi^{(2)}_{xyy} & 0 & \chi^{(2)}_{xyz} & \chi^{(2)}_{xzy} & \chi^{(2)}_{xzx} & \chi^{(2)}_{xxz} & \chi^{(2)}_{xxy} & \chi^{(2)}_{xyx} \\ \chi^{(2)}_{yxx} & \chi^{(2)}_{yyy} & 0 & \chi^{(2)}_{yyz} & \chi^{(2)}_{yzy} & \chi^{(2)}_{yzx} & \chi^{(2)}_{yxz} & \chi^{(2)}_{yxy} & \chi^{(2)}_{xyx} \\ \chi^{(2)}_{zxx} & \chi^{(2)}_{zyy} & \chi^{(2)}_{zzz} & 0 & 0 & 0 & 0 & \chi^{(2)}_{zxy} & \chi^{(2)}_{zyx} \end{bmatrix}$$

C_3 symmetry enables $\chi^{(2)}_{xxx} = -\chi^{(2)}_{xyy} = -\chi^{(2)}_{yxy} = -\chi^{(2)}_{xyx} = \chi_1$ and $-\chi^{(2)}_{yxx} = \chi^{(2)}_{yyy} = -\chi^{(2)}_{xxy} = -\chi^{(2)}_{xyx} = \chi_2$. Since the propagation direction of the pump photons and generation photons are along with the z-axis, the light waves can be regarded as transverse wave without E_z. A linearly polarized pump light is considered, and the pump state can be expressed as,

$$|\psi\rangle_p = \begin{pmatrix} E_{xp} \\ E_{yp} \end{pmatrix} = \begin{pmatrix} \cos\theta E_0 \\ \sin\theta E_0 \end{pmatrix}$$

in which θ is the direction of linearly polarization respect to the x-axis. The state of generated twin photons can be expressed as,

$$|\psi\rangle_{s,i} = C\begin{pmatrix} E_xE_x \\ E_xE_y \\ E_yE_x \\ E_yE_y \end{pmatrix} = C\begin{pmatrix} \chi^{(2)}_{xxx}E_{xp} + \chi^{(2)}_{yxx}E_{yp} \\ \chi^{(2)}_{xxy}E_{xp} + \chi^{(2)}_{yxy}E_{yp} \\ \chi^{(2)}_{xyx}E_{xp} + \chi^{(2)}_{yyx}E_{yp} \\ \chi^{(2)}_{xyy}E_{xp} + \chi^{(2)}_{yyy}E_{yp} \end{pmatrix} = CE_0\begin{pmatrix} \chi_1\cos\theta - \chi_2\sin\theta \\ -\chi_2\cos\theta - \chi_1\sin\theta \\ -\chi_2\cos\theta - \chi_1\sin\theta \\ -\chi_1\cos\theta + \chi_2\sin\theta \end{pmatrix}$$

For $\theta_1 = arctan\left(\frac{\chi_1}{\chi_2}\right)$, we obtain $\chi_1\cos\theta_1 - \chi_2\sin\theta_1 = 0$, and then the twin-photon state can be expressed as,

$$|\psi\rangle_{s,i} = -C(\chi_2\cos\theta_1 + \chi_1\sin\theta_1)\begin{pmatrix} 0 \\ 1 \\ 1 \\ 0 \end{pmatrix}$$

which is the maximally entangled Bell state $1/\sqrt{2}(|HV\rangle + |VH\rangle)$.

For $\theta_2 = arctan\left(-\frac{\chi_2}{\chi_1}\right)$, we obtain $\chi_2\cos\theta_2 + \chi_1\sin\theta_2 = 0$, and then the twin-photon state can be written as,

$$|\psi\rangle_{s,i} = C(\chi_1\cos\theta_2 - \chi_2\sin\theta_2)\begin{pmatrix} 1 \\ 0 \\ 0 \\ -1 \end{pmatrix}$$

corresponding to Bell state $1/\sqrt{2}(|HH\rangle - |VV\rangle)$.

Therefore, using linearly polarized pump light with an angle of θ_1 and θ_2, C3 symmetric nonlinear crystals can produce twin photons in two Bell states. θ_1 and θ_2 have the relationship of $\theta_2 = \theta_1 + \pi/2$. Specifically, for C_{3v} symmetric crystals, $\chi_1 = 0$, $\theta_1 = 0$, $\theta_2 = \pi/2$. For D_3 symmetric crystals, $\chi_2 = 0$, $\theta_1 = \pi/2$, $\theta_2 = 0$.

5. Evaluation of coherence length

The coherence length L_{coh} is calculated with the experimentally measured refractive indices of WS_2. It is worth noting that the refractive indices of the 3R phase are unclear, so we used the published data collected from 2H-WS_2[1]. L_{coh} can be calculated by,

$$L_{coh} = \frac{\lambda_\omega}{4(n_{2\omega} - n_\omega)}$$

where λ_ω is the fundamental wavelength, n_ω and $n_{2\omega}$ denote the refractive indices at fundamental and SHG wavelengths, respectively. In our experiments, the refractive indices are 4.306 and 3.903 at wavelengths of 457 nm and 914 nm, respectively, yielding an L_{coh} of 567 nm. Therefore, the phase-matching condition is fulfilled for 3R-WS_2 with a thickness of 350 nm.

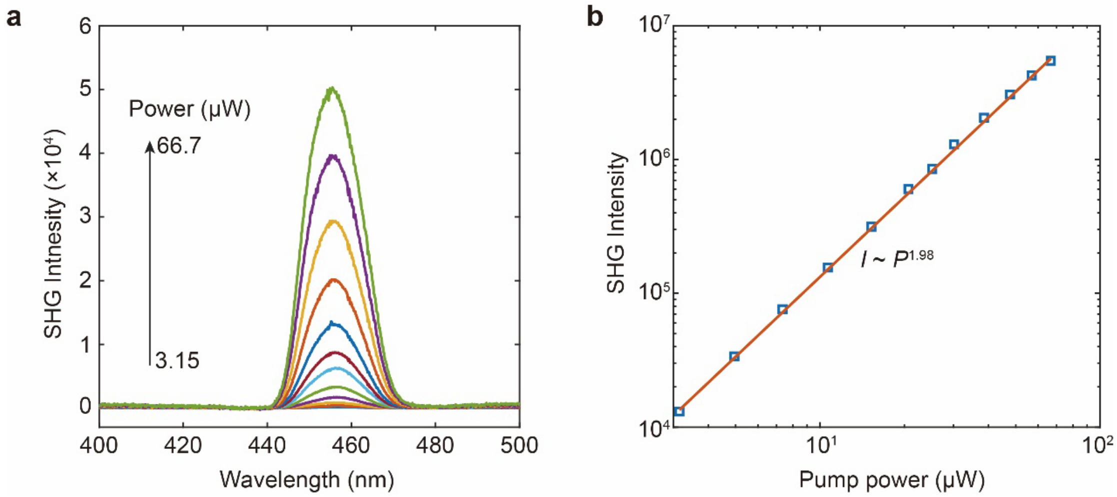

Fig. S1 | Power-dependent SHG measurements of 3R-WS_2. a, SHG spectra under pump powers ranging from 3.15 to 66.7 μW. **b**, Integrated SHG intensity as a function of pump power. A power law increasement of SHG intensity can be obtained with a coefficient of 1.98, indicating the SHG process in 3R-WS_2.

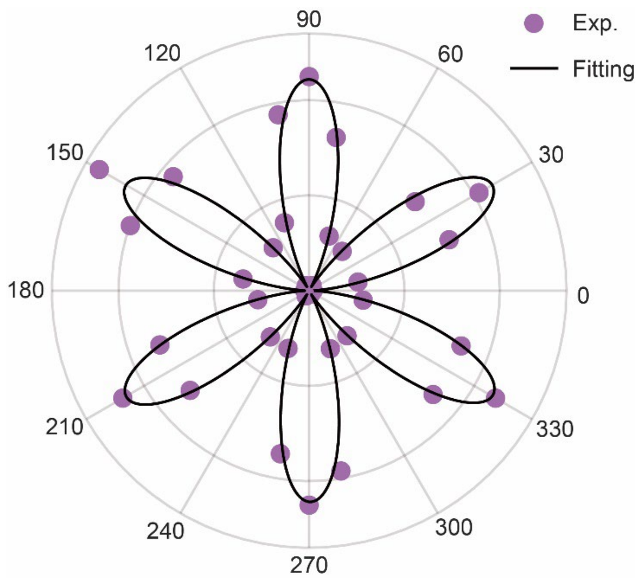

Fig. S2 | SHG intensity as a function of linear-polarization angle in 3R-WS_2. The experimental data can be well fitted by Eq. (6), in line with C_{3v} lattice symmetry in 3R-WS_2.

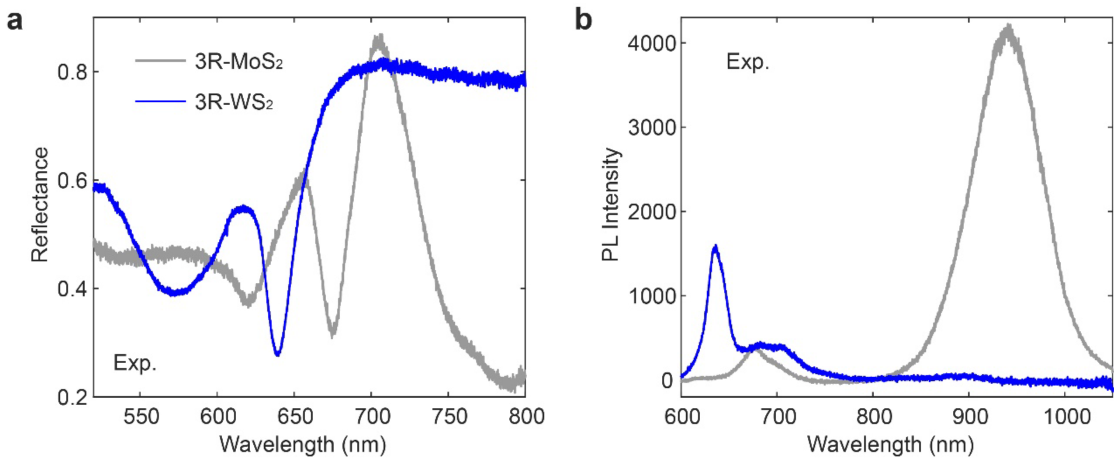

Fig. S3 | Reflectance (**a**) and PL (**b**) spectra of 3R-MoS_2 and 3R-WS_2.

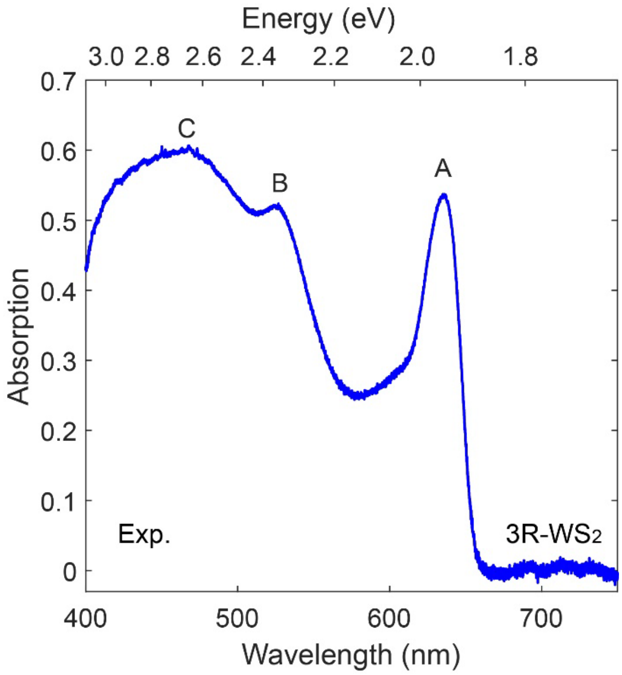

Fig. S4 | Absorption spectrum of 3R-WS_2.The absorption spectrum is obtained on a 60 nm flake by measuring transmittance T and reflectance R. The absorption A is then calculated by $A = 1 - R - T$. The A and B peaks correspond to excitonic transitions at the K and K' valleys, while the C peak can be attributed to transitions in a region of high density of states enabled by the 'band nesting' effect.

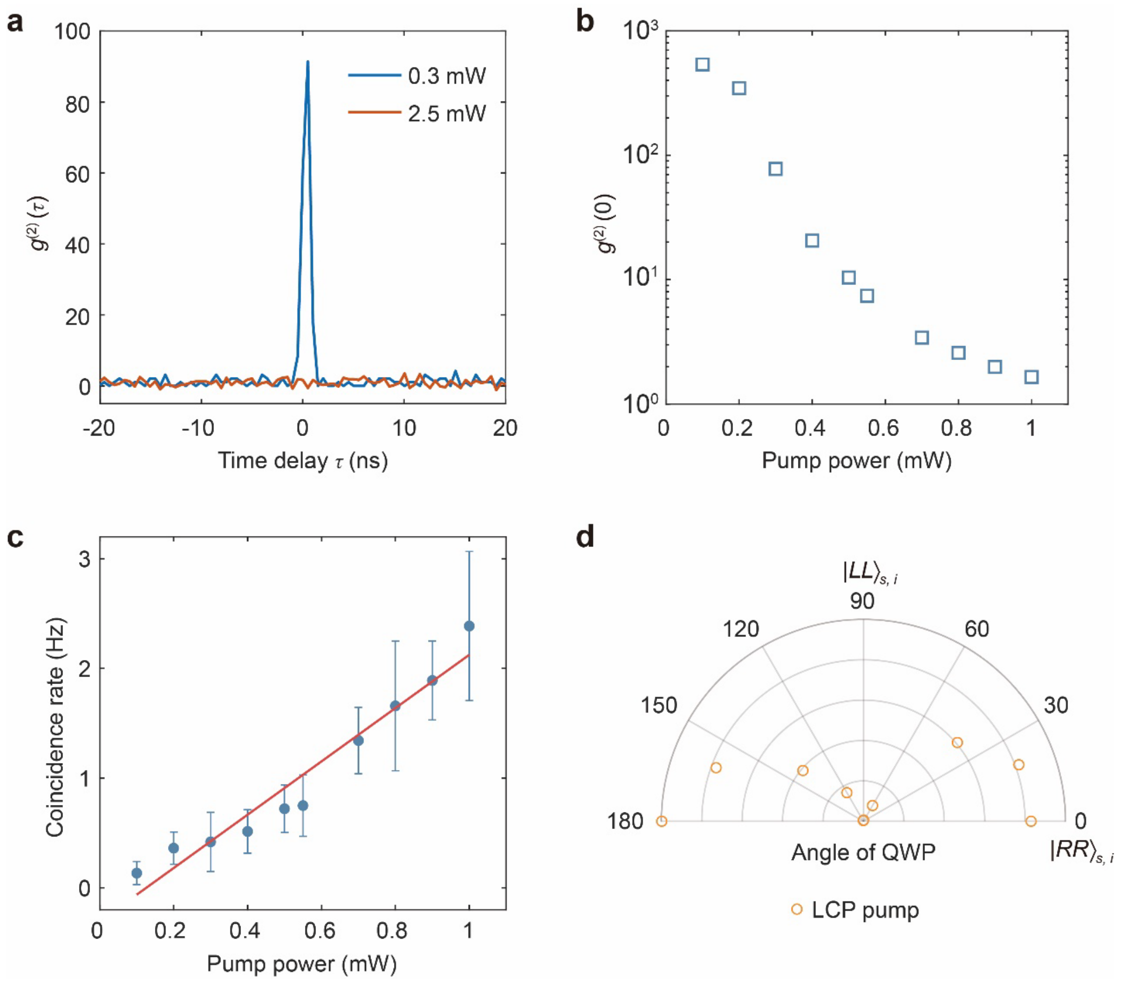

Fig. S5 | SPDC measurements in 3R-MoS2. **a**, Representative $g^{(2)}$ (τ) of 3R-MoS_2 under pump power of 0.3 mW and 2.5 mW. A 457 nm continuous-wave laser is employed to pump photon pairs centered at 914 nm. **b**, Pump-power dependent $g^{(2)}$ (0) of 3R-MoS_2, reflecting the degradation of quantum correlations with the rise of PL background. **c**, Coincidence rate as a function of pump power of 3R-MoS_2. **d**, Circular polarization analysis of photon pairs. A left-handed polarized pump is employed, and coincidence rate is recorded at different angles of quarter-wave plates.

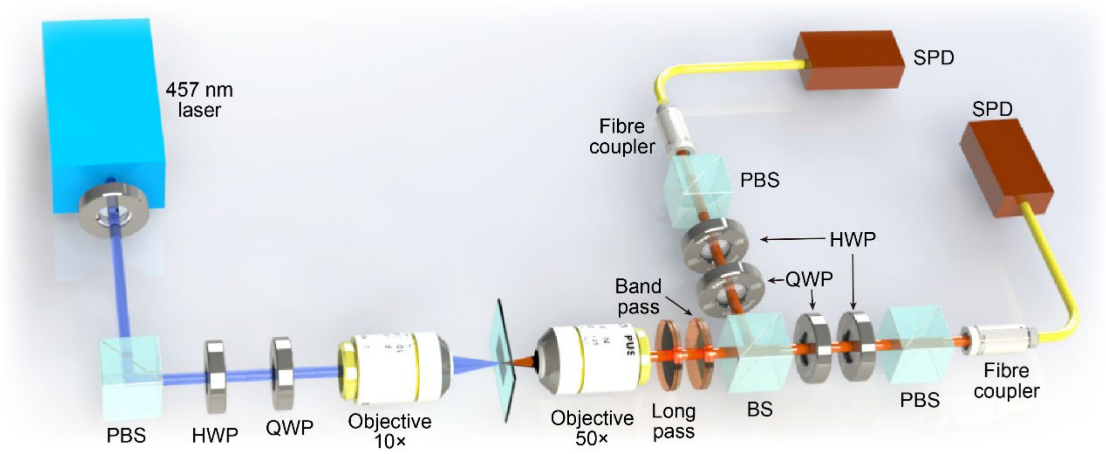

Fig. S6 | Scheme of experimental setup for quantum-state tomography. PBS, polarizing beam splitter; HWP, half-wave plate; QWP, quarter-wave plate; BS, beam splitter; SPD, single-photon detector. To filter out pump light, a long-pass filter at 900 nm and a band-pass filter with a center wavelength at 925 nm and a linewidth of 50 nm are employed.

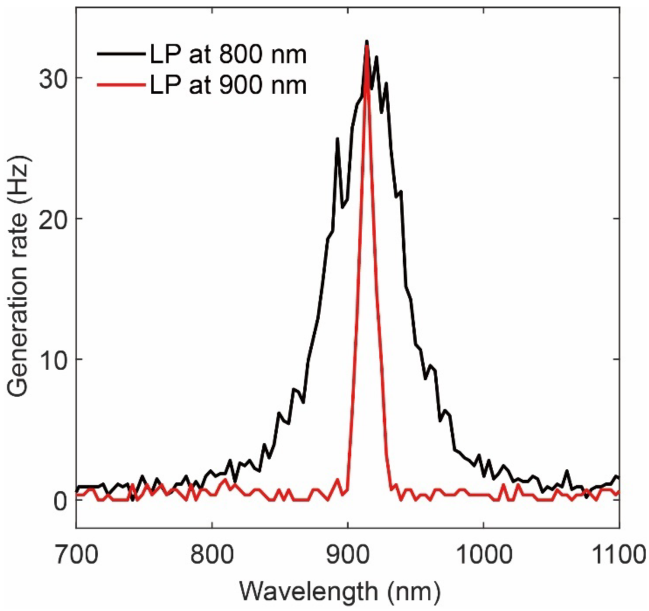

Fig. S7 | SPDC spectra of 3R-WS_2 under 457 nm pump. Two spectra are collected using long-pass filters at 800 nm and 900 nm, respectively. The spectra were measured according to the method in Ref. 2. The shapes of the spectra were modulated by the rapidly declining efficiency of the detectors for longer wavelength at near-infrared.

Table S1 | The state-of-the-art polarization-entangled photon-pair sources based on thin-film quadratic nonlinear materials.

Source	Path length	Entangle-ment	λ (nm)	Fidelity	CAR	Rate (Hz)	Rate (Hz mW^{-1})	Ref
3R-WS_2	350 nm	Polarization	914	0.95 0.93	820	31.1	1.71	This work
3R-MoS_2	285 nm	Polarization	1576	0.96 0.84	8.9±5.5	0.2	8.0×10^{-3}	3
$NbOCl_2$	150 nm	No	808	-	25	86	1.46	4
GaP	400 nm	Polarization	1276	-	-	4	6.7×10^{-2}	5
LN meta	680 nm	No	1576	-	361	5.4±0.1	7.7×10^{-2}	6
GaAs meta	500 nm	No	1450	-	9.5±1.1	0.07	7.4×10^{-3}	7
GaAs NWs	L = 5 μm D = 450 nm	No	1550	-	50	0.05	3.3×10^{-3}	8

Coincidence-to-accidental ratio (CAR), lithium niobate (LN), metasurfaces (meta), nanowires(NWs).

Supplementary References

1. Zotev, P. G. *et al.* Van der Waals Materials for Applications in Nanophotonics. *Laser & Photonics Reviews* **17**, 2200957 (2023).
2. Santiago-Cruz, T., Sultanov, V., Zhang, H., Krivitsky, L. A. & Chekhova, M. V. Entangled photons from subwavelength nonlinear films. *Opt. Lett.* **46**, 653–656 (2021).
3. Weissflog, M. A. *et al.* A Tunable Transition Metal Dichalcogenide Entangled Photon-Pair Source. Preprint at https://doi.org/arXiv:2311.16036 (2023).
4. Guo, Q. *et al.* Ultrathin quantum light source with van der Waals $NbOCl_2$ crystal. *Nature* **613**, 53–59 (2023).
5. Sultanov, V., Santiago-Cruz, T. & Chekhova, M. V. Flat-optics generation of broadband photon pairs with tunable polarization entanglement. *Opt. Lett.* **47**, 3872–3875 (2022).
6. Santiago-Cruz, T. *et al.* Photon pairs from resonant metasurfaces. *Nano Lett.* **21**, 4423–4429 (2021).
7. Santiago-Cruz, T. *et al.* Resonant metasurfaces for generating complex quantum states. *Science* **377**, 991–995 (2022).
8. Saerens, G. *et al.* Background-free near-infrared biphoton emission from single gaas nanowires. *Nano Lett.* **23**, 3245–3250 (2023).